Author(s): Zubiaga, A. & Garcia, J. A. & Plazaola, F. & Tuomisto, Filip & Zuniga-Perez, J. & Munoz-Sanjose, V.

Title: Positron annihilation spectroscopy for the determination of thickness and defect profile in thin semiconductor layers

Year: 2007

Version: Final published version

Please cite the original version:

Zubiaga, A. & Garcia, J. A. & Plazaola, F. & Tuomisto, Filip & Zuniga-Perez, J. & Munoz-Sanjose, V. 2007. Positron annihilation spectroscopy for the determination of thickness and defect profile in thin semiconductor layers. Physical Review B. Volume 75, Issue 20. 205305/1-10. ISSN 1098-0121 (printed). DOI: 10.1103/physrevb.75.205305

Positron annihilation spectroscopy for the determination of thickness and defect profile in thin semiconductor layers

A. Zubiaga,* J. A. García, and F. Plazaola
Fisika Aplikatua II & Elektrika eta Elektronika Saila, Euskal Herriko Unibertsitatea, P.K. 644, 48080 Bilbao, Spain

F. Tuomisto
Laboratory of Physics, Helsinki University of Technology, P.O. Box 1100, 02015 TKK, Espoo, Finland

J. Zúñiga-Pérez and V. Muñoz-Sanjosé
Departament de Fisica Aplicada i Electromagnetisme, c/ Doctor Moliner 50, E-46100 Burjassot (Valencia), Spain
(Received 19 September 2006; revised manuscript received 22 February 2007; published 3 May 2007)

We present a method, based on positron annihilation spectroscopy, to obtain information on the defect depth profile of layers grown over high-quality substrates. We have applied the method to the case of ZnO layers grown on sapphire, but the method can be very easily generalized to other heterostructures (homostructures) where the positron mean diffusion length is small enough. Applying the method to the ratio of *W* and *S* parameters obtained from Doppler broadening measurements, *W*/*S* plots, it is possible to determine the thickness of the layer and the defect profile in the layer, when mainly one defect trapping positron is contributing to positron trapping at the measurement temperature. Indeed, the quality of such characterization is very important for potential technological applications of the layer.

DOI: 10.1103/PhysRevB.75.205305 PACS number(s): 68.55.Jk, 68.55.Ln, 78.70.Bj

I. INTRODUCTION

In the last years the positron annihilation technique has become a fundamental technique for studying vacancy-type defects in wide-gap semiconductors, as GaN or ZnO.[1–3] Using monoenergetic positrons the penetration depth in the sample can be controlled, and this has opened a field of great interest for studying thin layers.[4–7] Thin layers are habitually studied by Doppler broadening of the positron annihilation radiation using *S* and *W* parameters, the annihilation intensity with low- and high-momentum electrons, respectively. They can be represented in a *W*/*S* plot, where positrons annihilating from a given defect and from bulk define a straight line characteristic of the defect in that material. Therefore, *W*/*S* plots are very valuable for defect identification.[8]

Very recently slow positron experiments have been performed in ZnO layers grown over sapphire.[7] Their *W*/*S* plots show curves with cusps corresponding to the minimum concentration of the defect. All measured cusp values fall within a straight line whose slope is indicative of the presence of the same zinc-vacancy-related defect in the layers. Even though the experimental data are very rich, only the position of the cusps in the *W*/*S* plot was used in the analysis and the vacancy concentration within the layer was obtained. However, it will be shown that further information can be extracted from a detailed analysis of the measured *W*/*S* plots.

In this sense and in order to obtain as much information as possible from *W*/*S* plots, we propose a method for determining the defect profile and the film thickness in layers grown over a substrate. The method has been applied to the study of ZnO layers grown on sapphire, but the same approach can be used in other layer/substrate semiconductor heterostructures (homostructures) for obtaining more information about the defect profile. Another important feature of the method is the determination (nondestructively) of the layer thickness. The measurement of layer thicknesses in heterostructures is not always an easy task. A common way to obtain this thickness, nondestructively, is to determine it indirectly through the growth rate. Nevertheless, more accurate thickness determinations usually require the use of experimental techniques, which can destroy the heterostructure.

II. EXPERIMENT

ZnO layers were grown by metal organic chemical vapor deposition (MOCVD) on sapphire substrates of different orientations and with different thicknesses; see Table I. For more details on the MOCVD growth see Munuera *et al.*[9] Scanning electron microscope (SEM) equipment (JEOL6400) was used for direct experimental thickness measurements. The error of the thickness measured by SEM corresponds to the difference between values determined at different positions along each sample.

TABLE I. Description of the studied layers: orientation of sapphire substrates on which the layers were grown, cusp, abandon point, and 50% percentage point in each sample (see main text for definitions).

Sample	Substrate plane	Cusp (nm)	Abandon point (±30 nm)	50% point (nm)
1	*C* (0001)	120	240	480
2	*M*(10-10)	100	240	440
3	*A*(11-20)	70	160	330–380
4	*C*(0001)	240	440	800–860
5	*C*(0001)	240	400	870
6	*R*(1-102)	240	360	670–900
7	*R*(1-102)	160	330	550–600

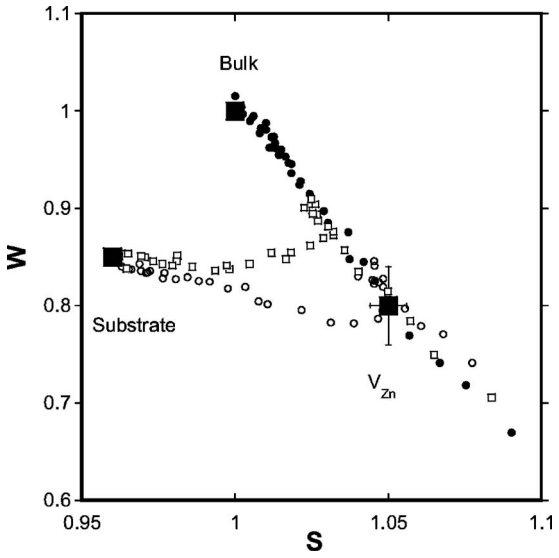

FIG. 1. *W*/*S* plot of the ZnO reference sample (solid circles) and two layers grown over sapphire (sample 1, open circles, and sample 7, squares). Bulk and V_{Zn} mark the *W*/*S* parameters of positrons annihilating from the delocalized ZnO state and from zinc vacancies, respectively. Substrate refers to the *W*/*S* parameters of positrons annihilating in sapphire.

Positron experiments were performed at room temperature with a monoenergetic positron beam. The energy of the beam was varied in the 0–38-keV energy range. The Doppler broadening of the annihilation radiation was measured using a Ge detector with an energy resolution of 1.24 keV at 511 keV. To characterize the spectra, the energy windows used were $|E_\gamma - 511\ \text{keV}| < 0.8\ \text{keV}$ $(p_L/m_0c \leq 3\times10^{-3}$, where m_0 is the electron mass) for the *S* parameter and $2.9\ \text{keV} \leq |E_\gamma - 511\ \text{keV}| \leq 7.4\ \text{keV}$ $(11\times10^{-3} \leq p_L/m_0c \leq 29\times10^{-3})$ for the wing *W* parameter. An as-grown ZnO bulk sample whose vacancy concentration is very low, and which at room temperature only presents annihilation in the bulk with an average positron lifetime of 171 ps[2], was used as the reference sample.

III. RESULTS

The Doppler broadening spectroscopy technique gives information about the electronic momentum distribution at the annihilation site. The momentum distribution is different when the positron is in the delocalized state or trapped at a vacancy. In the latter, the distribution is narrower because there is a lack of core electrons of high momentum. Momentum annihilation parameters (*S* and *W* parameters) of positrons trapped at vacancy-type defects change with respect to the annihilation from the delocalized state. Figure 1 shows the *W*/*S* plot of a bulk ZnO sample (reference sample) and two (ZnO layer+sapphire substrate) heterostructures. The reference sample has a negligible concentration of defects, and it shows a straight line (solid circles in Fig. 1) where the upper left corner corresponds to the *W* and *S* parameters of positrons annihilating from delocalized states in bulk ZnO.[2] The straight line indicates that there are only two states where positrons annihilate. At very low implantation energies positrons preferentially annihilate at surface states (bottom right corner in Fig. 1), but at high implantation energies almost all positrons are annihilating from delocalized states in the bulk of ZnO.

Figure 1 also shows the totally different behavior presented by ZnO layers grown on sapphire. At very low implantation energies positrons are preferentially annihilating from surface states (bottom right corner in Fig. 1). At higher implantation energies the *W*/*S* plot follows a straight line toward a cusp whose maximum depends on the measured layer. At implantation energies higher than the one corresponding to the cusp the measured values do not follow the previous straight line, and they tend toward a new position. The position obtained at the highest implantation energies corresponds to positron annihilation at the bulk of the sapphire substrate. Figure 1 shows, too, *W*/*S* points corresponding to positrons annihilating from delocalized states in ZnO (bulk), from the substrate (substrate), and from zinc vacancies in ZnO (V_{Zn}). The parameters corresponding to positron annihilation from zinc vacancies have been estimated from simultaneous lifetime and Doppler measurements in an electron-irradiated single crystal ZnO.[2]

All the measured cusp values fall within a straight line in the *W*/*S* plots. It joins the ZnO bulk and zinc vacancy characteristic values, and its slope amounts to −3.67(5), indicating that the zinc vacancy is responsible for the trapping at the ZnO layers presented in this work.[5] From now on, we will call it the "vacancy line." The point where the *W*/*S* curve leaves the vacancy line will be called the "abandon point." Positron energies are larger at the abandon point than in the cusp.

IV. DISCUSSION

In the following the positron implantation process will be analyzed. Characteristics such as the positron penetration and its implantation depth, the positron diffusion length (in the layer and the substrate), and its probability distribution after the diffusion have been considered in order to extract more information from *W*/*S* plots like in Fig. 1. The analysis of the implantation and the diffusion process will allow one to obtain further information about the quantity and the distribution of the trapping centers in the sample.

A. Positron implantation profile and penetration depth

The energy *E* of the implanted positrons has been varied between 0 and 38 keV in the experiments. The positron implantation energy and the mean implantation depth of the positron into the sample, $\langle z\rangle$, are related by the equation $\langle z\rangle = BE^n/\rho$, where ρ is the material density (5.6 g/cm^3 for ZnO) and *n* and *B* are 1.6 and 4×10^{-6} g/cm^{-2} keV$^{-1.6}$, respectively.[8] The stopping profile of positrons penetrating the sample is described by the Makhovian function

$$I(z) = \frac{2z}{z_0^2} e^{-(z/z_0)^2}, \tag{1}$$

where z_0 is related to the mean penetration depth by $\langle z\rangle = 0.886 z_0$ (see Saarinen *et al.*[8] and references therein).

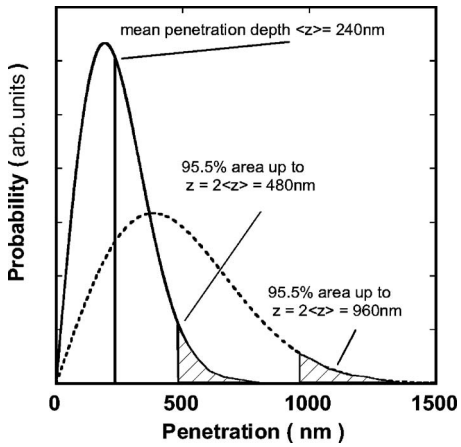

FIG. 2. Shape of the positron implantation profile for two different mean penetration depths.

Figure 2 shows the shape of the positron stopping profile for two particular mean penetration depths $\langle z\rangle = 240$ and 480 nm, which correspond to implantation energies [Eq. (1)] of 3.8 keV and 5.8 keV, respectively. The stopping profile function extends from the surface towards the inner part of the sample. The larger the mean implantation depth is, the deeper the stopping profile extends inside the sample. For instance, for a layer 1000 nm thick practically all positrons with $\langle z\rangle = 250$ nm are implanted inside the layer, but for $\langle z\rangle = 500$ nm they can cross the layer/substrate interface. Thus, for larger penetration energies or mean penetration depths, Doppler parameters of the annihilated positrons can provide information not only on the layer, but on the substrate too. The long tail of the stopping profile extends towards large depths; nevertheless, the probability of implantation at depths larger than $2\langle z\rangle$ is only 4.5%. Neglecting this 4.5% probability of the implantation profile tail above $2\langle z\rangle$, the resulting function is quasisymmetrical and centered at the mean penetration depth value $\langle z\rangle$. The maximum penetration depth defined in this way is $2\langle z\rangle$, twice the mean penetration depth.

When positrons have enough energy to enter the substrate, the stopping profile will be different from that given by Eq. (1). At the interface position they have lost part of the initial kinetic energy. In addition, the stopping profile at larger depths than that of the interface will depend on the substrate density. The change in the positron implantation probability should be smooth if no considerable trapping is observed in the interface.

The proposed stopping profile is presented in Eq. (8). It depends on the substrate density and the energy loss while traveling up to the interface along the layer. An effective depth $d+\rho_1/\rho_0(z-d)$ is defined, and it is continuum and smooth at the interface. If both materials have similar density values, like in the ZnO/sapphire heterostructures, the shapes of the stopping profiles are qualitatively similar, but the implantation profile will have a slightly longer tail inside the sapphire, since its density is slightly lower than that of ZnO.

We must consider the mean diffusion length (L_{diff}) of the positron in the layer and in the substrate for a correct interpretation of the results. Positrons diffuse along the material until they get trapped at a defect or they annihilate in the bulk. Considering the diffusion equation[8] and using the VEPFIT program,[10] we can adjust the variation of the S parameter versus the implantation energy. Fitting the studied samples with VEPFIT gives values of 22 ± 5 nm and 80 ± 10 nm for the positron mean diffusion length in the layer and in the substrate, respectively. When compared with the mean penetration depth, it is readily observed that L_{diff} in the ZnO layer is much smaller than the layer thicknesses considered in this work, and we can neglect it in the following discussion. Thus, we can consider $2\langle z\rangle$ as the maximum penetration depth for the positrons in the layer.

Figure 3 compares W and S parameters plotted versus implantation energy and the corresponding W/S plot. The singularity of the marked points is clearly seen in the W/S curve.

B. Method to determine semiconductor layers thicknesses

Returning to the W/S plot in Fig. 1 we can see that at very low implantation energies (and, hence, low penetration depths) positrons are mainly annihilating at surface states (bottom right corner in Fig. 1). As the implantation energy is increased, the W/S plot tends towards a cusp. The cusp position corresponds to the maximum of the W parameter, and the relative minimum of the S parameter versus implantation energy and is characteristic of each measured layer; see Table I. The cusp mean implantation depths range between 70 and 240 nm, and the corresponding maximum penetration depths are, as we will demonstrate later, smaller that the layer thickness in all samples. This maximum can be easily inferred from Figs. 1 and 3.

At implantation energies higher than the one corresponding to the cusp but maximum penetrations depths shorter than the layer thickness, the W/S measured values still lay over the "vacancy line." In the studied samples the abandon point is attained for mean penetration depths between 160 ± 30 nm and 440 ± 30 nm (see Table I). Abandoning the "vacancy line" indicates that positrons are starting to annihilate from another state, different to the ones that gave the "vacancy line" (delocalized state at ZnO and zinc vacancy). This indicates that for energies larger than the one corresponding to the abandon point positrons start to annihilate outside the layer. Taking into account this fact and the shape of the implantation profile (Fig. 2), the abandon point must correspond to mean penetration depths in the order of half the sample thickness. Therefore, under these conditions the stopping profile function extends from the surface of the layer up to the interface between the layer and the substrate; see Fig. 1 and Table I. For larger energies, positrons cross the interface and start annihilating inside the substrate.

The previous discussion indicates that a simple and nondestructive way for determining the thickness of a layer grown on a substrate consists on determining the abandon point in the W/S plot. The thickness of the layer corresponds to twice its mean implantation depth at the abandon point ($2*\langle z_{abandon}\rangle$). Table II shows the thickness of the studied samples obtained by two different methods: the nondestructive method based on determining the abandon point, as in-

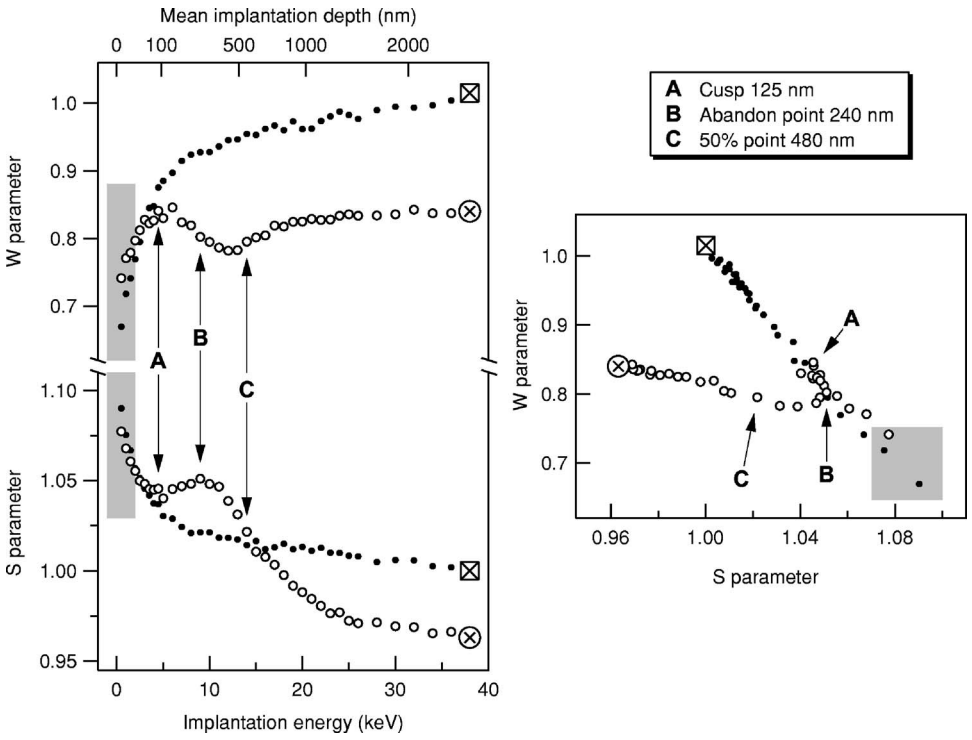

FIG. 3. Comparison of the *W* and *S* parameters versus the positron penetration depth for sample 1 (left graph) and the corresponding *W*/*S* curve (right graph). The most relevant parameters of the layer are represented: the cusp position (*A*), the abandon point (*B*), and the 50% percentage point (*C*) (see the text for more details). The surface state (shadowed area), the bulk reference value (crossed square), and the substrate value (crossed circle) are also shown.

troduced in the present work, and a destructive one based in scanning electron microscope images of the cleaved samples. Very good agreement is attained between both methods. Moreover, increasing the number of *W*/*S* points measured at energies around the abandon point will improve the resolution in measurements of the layer width. In Sec. IV E, layer thickness values obtained using a more elaborated analysis are presented.

C. Method for the determination of the defect profile in the layer

Between the cusp position and the abandon point the *W*/*S* curve tends towards the zinc vacancy values, indicating that the concentration of zinc vacancies close to the interface is significant. At higher energies, the probability of positrons annihilating in the substrate starts to be significant and the measured *W* and *S* values tend to the annihilation values of sapphire.

As already stated, the *W*/*S* point where the positron leaves the straight line is related to the concentration of vacancies close to the interface. This value corresponds to a mean penetration depth equal to half the sample width. The distance in the *W*/*S* plot between the cusp position and the abandon point is proportional to the variation of the zinc vacancy concentration, as we will show later. From Figs. 1 and 3 it can be inferred that the vacancy concentration is minimum inside the layer at depths lower than one-third of the layer thickness and increases up to the interface—that is, for mean penetrations around half of the thickness of the samples.

For mean penetration depths larger than half of the layer thickness, the probability that positrons annihilate at the interface and inside the substrate increases, and from this point on the results cannot be easily separated into the different contributions. In Fig. 3 the point where the *W*/*S* plot reaches the minimum *W* value for sample 1 after abandoning the vacancy line is indicated by an arrow, and it corresponds to a mean penetration depth of 480 nm. Although this point is outside the straight line, it keeps some information on the annihilation parameters of the layer but with some influence from the substrate. The corresponding mean penetration depth is close to the thickness of the layer, so it brings information about the annihilation characteristics near the interface. The above analysis can be extended to the rest of the samples. In the following we will analyze this general behavior in order to understand it and to obtain further information from these data.

The method we propose for the determination of the defect profile in semiconductor layers grown heteroepitaxially, can be generalized to other heterostructures (homostructures) if they fulfill the following conditions.

TABLE II. Layers thickness measured by two different methods: scanning electron microscopy and by the abandon point method developed in this work.

Sample	SEM (nm)	2×(abandon point) (±60 nm)
1	540±50	480
2	410±40	480
3	450±70	320
4	860±150	880
5	660±70	660
6	760±50	720
7	630±60	660

(i) The positron diffusion length is much smaller than the layer thickness.

(ii) The layer has only one defect trapping positron at the measurement temperature.

(iii) Positron annihilation in the substrate comes from only one state.

The three conditions are not very restrictive and the method can be, thus, employed in many systems.

1. Definitions in the W, S plane

We can divide the W/S curves of all the samples in the W/S plot into three different zones according to the positron implantation (and annihilation) depths into the sample: the layer zone, which corresponds to the "vacancy line" (all positrons annihilate within the layer), the intermediate zone, which starts at the abandon point and extends up to the third zone (positrons annihilate from both the layer and the substrate), and the third zone, which is representative of the W/S substrate values (most of the positrons annihilate at the substrate). In Fig. 1 these three zones can be easily distinguished.

The experimental W/S value corresponding to the sapphire substrate can be obtained in a straightforward and accurate way measuring W and S for a bare sapphire wafer used for growing ZnO on it or by implanting the positrons first through the substrate and measuring W and S parameters for penetration depths far from the sapphire-ZnO layer interface depth. However, the W/S value corresponding to the sapphire substrate can be obtained, as in the present case, where positrons are implanted first through the ZnO layer, from the experimental results when the penetration depth of the positron beam attains its maximum value—that is, 2400 nm in the present work. In this case the stopping profile function or the annihilation probability of the positron in the layer is 12.7% for a layer 1000 nm thick or only 3.3% for a layer 500 nm thick. If we use the W/S value determined in the thinner layers for a mean penetration depth of 2400 nm, the error of the W and S parameters belonging to the substrate will be smaller than 5%.

On the other hand, all points in the W/S plot are enclosed by three lines, which establish the limits of the W/S plots. These lines are the "vacancy line," the "bulk line," which runs from the ZnO bulk to the substrate W/S values, and the "saturation line," which joins the zinc vacancy and the substrate W/S values; see Fig. 4.

From now on, individual contributions to the W and S parameters will be written as (W/S) and contributions from the layer and the substrate are accounted for with subscripts *ly* and *sb*, respectively. In a heterostructure formed by a layer with a constant vacancy distribution over the substrate, the (W/S) value of the heterostructure can be deduced from the following equations:

$$(W/S)_{total} = (W/S)_{ly}[0,d]P_{ly} + (W/S)_{sb}[d,D=\infty]P_{sb}, \quad (2)$$

$$(W/S)_{ly} = (W/S)_{bulk}\eta^{eff}_{bulk}(z) + (W/S)_{VZn}\eta^{eff}_{VZn}(z), \quad (3)$$

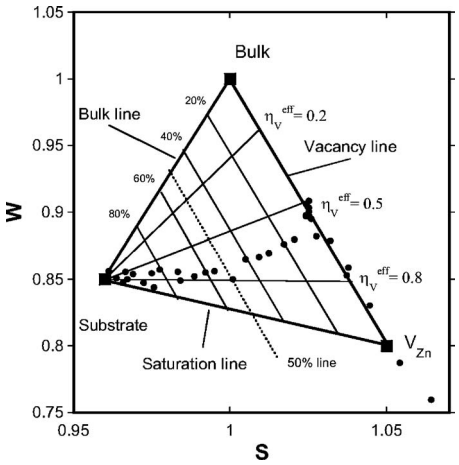

FIG. 4. W/S plane presenting percentage lines, effective constant trapping fraction lines, and several lines defined in the main text. The experimental data points correspond to sample 6.

where $(W/S)_{bulk}$ corresponds to the annihilation parameters for the bulk reference sample and $(W/S)_{VZn}$ to saturated trapping at zinc vacancies. P_{ly} and P_{sb} correspond to the annihilation probability in the layer and substrate, respectively. D and d are the layer and substrate thicknesses, respectively.

η^{eff}_{VZn} is the effective trapping fraction at zinc vacancies. It fulfills a relation similar to the trapping fraction and allows for nonconstant trapping fractions

$$\eta^{eff} = \int_0^d \eta(z)I(z)dz, \quad (4a)$$

$$\eta^{eff}_{bulk}(z) + \eta^{eff}_{VZn}(z) = 1. \quad (4b)$$

Bearing in mind the above equations, we can define the percentage lines (% lines), which represent the percentage of positrons implanted at the substrate, as in Fig. 4. Each line corresponds to W and S parameters with a particular proportion of positrons being implanted in the substrate. We can draw, for instance, the 50% line, which means that P_{sb}=0.5 (the probability of an implanted positron to annihilate in the substrate is 0.5). The mean penetration depth for points in this line corresponds approximately to the thickness of the layer—that is, twice that of the abandon point (see Table I). The percentage lines extend between the "bulk line" and the "saturation line" and run parallel to the "vacancy line"; see Fig. 4.

We can also define the constant trapping fraction lines (η^{eff}_{VZn}), which join points with the same effective trapping fraction. They extend between the "vacancy line" and the substrate value. The η^{eff}_{VZn} trapping fraction is proportional to the zinc vacancy concentration (see next section).

As a first step, we can deduce the defect profile of a particular layer by the (P_{sb}, η^{eff}_{VZn}) pair of values corresponding to each experimental point, as shown in Fig. 5. For any experimental point, the η^{eff}_{VZn} value and its associated penetration depth (P_{sb}) can be calculated and, using these values, the defect profile can be approximately obtained (see the inset in Fig. 5).

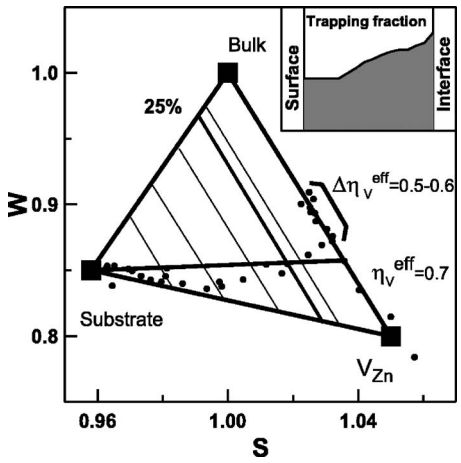

FIG. 5. Percentage line and effective constant trapping fraction line corresponding to a particular experimental point of sample 7. $\Delta\eta_V^{eff}$ indicates the effective trapping fraction value difference between the cusp and the abandon point in the layer. The inset shows the defect profile deduced from the experimental W/S plot of the layer.

2. Calculation of the W and S annihilation parameters as a function of penetration depth

The contribution to the experimental W and S values of the sample, $(W/S)_{total}$, using Eq. (2), can be expressed in a more general way as follows:

$$(W/S)_{total} = \int_0^d (W/S)_{ly} I(z)dz + \int_d^\infty (W/S)_{sb} I(z)dz, \quad (5a)$$

$$(W/S)_{ly} = (W/S)_{bulk} + [(W/S)_{VZn} - (W/S)_{bulk}]\eta_{VZn}(z), \quad (5b)$$

where $I(z)$ is the implantation profile or probability function along the whole sample, and $\eta_{bulk}(z)$ and $\eta_{VZn}(z)$ are the bulk and zinc vacancy trapping fractions in zinc oxide, respectively.

The ratio η_{VZn}/η_{bulk} is proportional to the defect concentration $C(V_{Zn}) = K\eta_{VZn}/\eta_{bulk}$, where $K = N_{at}\lambda_b/\mu$ is the proportionality constant. N_{at} is the atom density of the material, λ_b the annihilation rate at delocalized states, and μ the defect specific trapping rate. η_{VZn}/η_{bulk} is dimensionless, and it will be represented by the function $f(z)$. We can then write $\eta_{VZn} = f(z)\eta_{bulk}$, and taking into account that $\eta_{bulk}(z) + \eta_{VZn}(z) = 1$,

$$\eta_{VZn}(z) = \frac{f(z)}{1 + f(z)}. \quad (6)$$

The $(W/S)_{total}$ can be written as

$$(W/S)_{total} = (W/S)_{sb}\frac{\rho_0}{\rho_1}\frac{e^{-(d/z_0)^2}}{A} + (W/S)_{bulk}\frac{1 - e^{-(d/z_0)^2}}{A} + \int_0^d [(W/S)_{VZn} - (W/S)_{bulk}]\frac{f(z)I(z)}{1 + f(z)}dz \quad (7)$$

where $I(z)$ is

$$I(z) = \frac{2}{A}\begin{cases} \frac{z}{z_0^2}e^{-z^2/z_0^2}, & z < d, \\ \frac{z'}{z_0^2}e^{-z'^2/z_0^2}, & z, z' = d + \frac{\rho_1}{\rho_0}(z - d) > d, \end{cases} \quad (8)$$

where $z_0 = 40/\rho_0/0.886E^{1.6}$ (ZnO) and z' is an effective depth that takes into account the different density of the layer and the substrate. The A factor assures that $I(z)$ is a probability function normalized to unity and has the value:

$$A = 1 + \left(\frac{\rho_0}{\rho_1} - 1\right)e^{-(d/z_0)^2},$$

where ρ_0 and ρ_1 are the densities of the layer and the substrate, respectively. The distribution is smooth at the interface, and it depends on the density of the material and the energy of positrons like a Makhovian function.

If the density of the substrate is much larger than the layer one, most positrons will preferentially annihilate in the layer, independently of their energy. On the other hand, if the density of the substrate is much lower than the layer one, positrons with enough energy will enter easily into the substrate and the penetration depth will get largely increased. In the following we will consider that the densities of layer and substrate are similar and, therefore, the probability distribution in the substrate and in the substrate will be similar. In the analysis above we have estimated the expression for $I(z)$ in a simple way, but a more exact expression could be obtained from experimental measurements or Monte Carlo calculations.

In the next two subsections (Secs. IV C 3 and IV C 4) we will illustrate the calculation of the W/S parameters for two different zinc vacancy distributions: namely, a constant defect concentration and a linearly increasing one as an example for a nonconstant defect profile.

3. Defect profile of constant value

When the layer has a constant concentration of zinc vacancies along its thickness, $f(z) = f(0) = \text{const}$, and W and S parameters can be easily calculated. Let us take a value for $f(0)$ which leads to a value of 0.5 for η_{VZn} in Eq. (6). Plotting for this case Eq. (7) for different penetration depths $\langle z\rangle$, the representative W/S values will follow a line, the 0.5 effective constant trapping fraction line ($C1$ in Fig. 6). So, once the "vacancy line" in the W/S plot is abandoned for maximum penetration depths larger than the layer thickness, the W/S values will follow a straight line which joins the point where the line is abandoned and the W/S parameters representative of the substrate—that is, the effective trapping fraction lines defined before.

On the other hand, for a constant defect profile in the layer, Eq. (7) becomes

$$(W/S)_{total} = \frac{\rho_0}{\rho_1}\frac{e^{-(d/z_0)^2}}{A}(W/S)_{sb} + \frac{1 - e^{-(d/z_0)^2}}{A}[(W/S)_{bulk}\eta_{bulk} + (W/S)_{VZn}\eta_{VZn}], \quad (9)$$

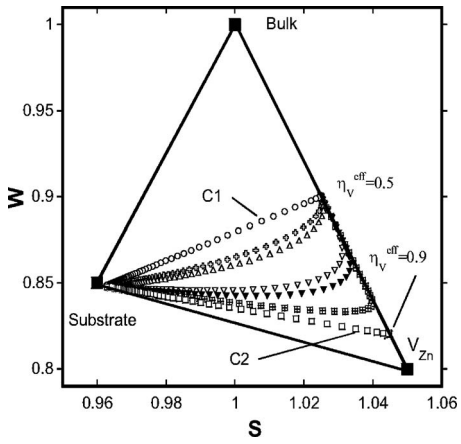

FIG. 6. Simulated W/S curves for different profiles detailed in Table III and Fig. 7: C1 (open circles), C2 (open squares), $L1$ (crossed squares), $L2$ (crosses), $J1$ (open downward triangles), $J2$ (open upward triangles), and JS (solid downward triangles).

$$(W/S)_{total} = \frac{\rho_0}{\rho_1}\frac{e^{-(d/z_0)^2}}{A}(W/S)_{sb} + \frac{1-e^{-(d/z_0)^2}}{A}(W/S)_{ly}, \tag{10}$$

$$(W/S)_{total} = (1-P_0)(W/S)_{sb} + P_0(W/S)_{ly}, \tag{11}$$

where P_0 is the probability of the positron to annihilate inside the layer. P_0 is obtained integrating the probability $I(z)$ from 0 to the entire layer thickness. Its value depends on the layer thickness, the densities of the layer and the substrate, and the positron implantation energy

$$P_0 = \frac{1-e^{(d/z_0)^2}}{1+(\rho_0/\rho_1-1)e^{(d/z_0)^2}}. \tag{12}$$

As expected, when the layer and the substrate have similar densities, the value of P_0 is similar to the layer value $1-\exp[-(d/z_0)^2]$.

4. Nonconstant defect profiles

Now we can perform the analysis of the W/S plot for a varying defect concentration distribution, for which we only need to know the vacancy concentration $f(z)$ or the trapping fraction η_{VZn} as a function of the sample depth. Using Eq. (7) we can calculate the evolution of the W/S parameters versus the implantation energy.

We need to solve the integral of Eq. (7) for the appropriate values of $f(z)$. The equation can be solved numerically for any distribution of zinc vacancies such as, for instance, a linear vacancy concentration distribution increasing from the layer surface, $\eta_{VZn}=0.5$, up to the interface, $\eta_{VZn}=0.9$ ($L1$ distribution in Table III and Fig. 7). Taking into account Eq. (6) this yields values of $f(z)=a+bz$, with $a=1$ and $b=0.016\ \text{nm}^{-1}$ for a layer of 500 nm. The result of the W/S trends for the two linear distributions that we have considered ($L1$ and $L2$ in Table III and Fig. 7) are presented in Fig. 6.

TABLE III. Characteristics of the defect profiles used to simulate W/S curves in Fig. 6. A scheme of these profiles can be found in Fig. 7.

	$C1$	$C2$	$L1$	$L2$	$J1$	$J2$	JS
η_{VZn} at surface	0.5	0.9	0.5	0.5	0.5	0.5	0.5
η_{VZn} at interface	0.5	0.9	0.9	0.9	0.9	0.9	0.99
Point of concentration change			surface	3/4th sample width	1/2th sample width	3/4th sample width	1/4th
							0.66
							0.82
							0.99
Number of steps					1	1	3
Step width					1/2th	1/4th	1/4th

The previously described calculation yields different W/S trends according to the assumed vacancy concentration profile. Figure 6 plots the W/S results for different vacancy concentration distributions, whose characteristics are summarized in Table III and shown in Fig. 7 and considering a sample 500 nm thick. The results for a constant distribution of zinc vacancies ($\eta_{VZn}=0.5$, $C1$ line in Fig. 6 and $\eta_{VZn}=0.9$, $C2$ line in Fig. 6) are identical to the qualitative prediction done before (see Sec. IV C 3).

Yet we have the tools for analyzing the experimental W/S trends of different ZnO layer samples grown on different sapphire substrate orientations. Figure 8 shows the experimental W/S trends for the studied samples. The effective trapping fraction can be estimated from the effective trapping fraction line cutting the experimental (W/S) value.

High energetic positrons are more sensitive to the vacancy content at the interface area than at the layer surface. So the different values of the integrated η_{VZn} trapping fraction give a qualitative indication of the vacancy gradient along the layer.

Comparing these results and those obtained from the analysis we have done above, a first approximate zinc va-

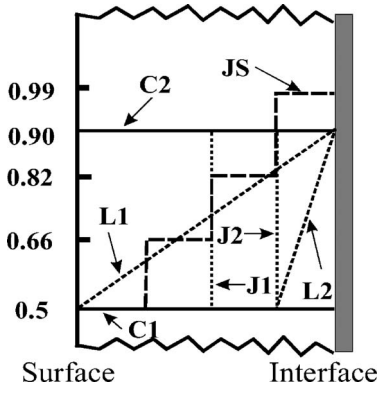

FIG. 7. Representation of the defect profiles explained in detail in Table III.

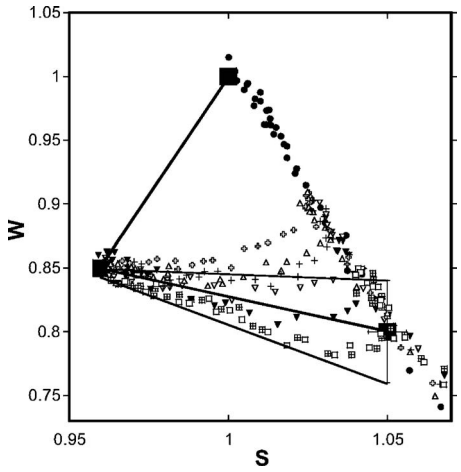

FIG. 8. *W*/*S* plane representing *W*/*S* plots of different measured layers: reference ZnO (solid circles), sample 1 (crossed squares), sample 2 (open downward triangles), sample 3 (solid downward triangles), sample 4 (open upward triangles), sample 5 (squares), sample 6 (bulky crosses), and sample 7 (crosses). Straight lines from the substrate *W*/*S* point to the borders of the errors bar of the *W*/*S* point of the zinc vacancy are drawn as a guide to the eyes.

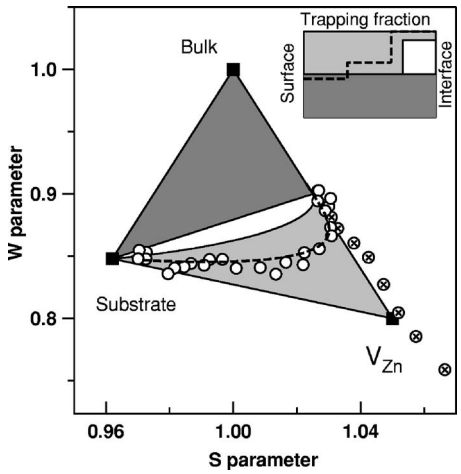

FIG. 9. *W*/*S* plane representing the areas enclosed by the "vacancy line," the "bulk line," and *W*/*S* curve simulated for the three different trapping fraction profiles shown in the inset: dark, dark+white and dark+white+gray. In addition, the fit of the sample 4 and the calculated trapping fraction are shown.

cancy distribution in the measured samples can be inferred. The experimental trend of sample 6 (bulky crosses in Fig. 8) is very similar to the simulated trend for a constant vacancy distribution along the layer thickness, with an increase in the concentration of zinc vacancies near the layer/substrate interface, as in the *L*2 situation. Sample 2 (downward triangles) presents a trend closer to the simulation with higher density of zinc vacancies as the "*J*1" case.

It can be seen that in all the samples after the *W*/*S* function reaches the cusp position, it abandons the "vacancy line" and, after arriving at the 50% line, it follows a linear trend from this point up to the *W*/*S* point of the substrate. This behavior is present in both the simulation and experimental results.

D. Relationship between the *W*/*S* plot area and the defect concentration

It would be very useful if just by inspecting the *W*/*S* plot a quick calculation of the total defect concentration in the layer could be carried out. When the vacancy content in the layer is large, the curve of the *W*/*S* plot is close to the unity effective trapping fraction line (saturation line) described above. On the other hand, when the vacancy content is negligible the curve of the *W*/*S* plot is near to the zero effective trapping fraction line (bulk line); see Fig. 6. Thus, the area enclosed by the "vacancy line," the "bulk line," and the *W*/*S* curve of the sample can be related to the total zinc vacancy content. Figure 9 presents the areas enclosed by the vacancy line, the bulk line, and the *W*/*S* curve simulated for three different trapping fraction profiles along the layer (see inset of Fig. 9): constant trapping fraction with $\eta=0.5$ (dark), step like (dark+white), and constant trapping fraction with $\eta=1$ (dark+white+gray). Sample 4 fitted using the procedure explained in the next section is also shown. The proportionality between the *W*/*S* plot area and the defect concentration is apparent. Indeed, there exists a linear relationship between the integrated trapping fraction inside the layer, for a constant vacancy distribution, and the area of the *W*/*S* plot. This can be easily inferred analytically using Eq. (7) and is shown by the solid line in Fig. 10.

In Fig. 10 the *W*/*S* areas for the vacancy distributions presented in Table III and Fig. 7 are shown. This figure shows too the deviation from the constant vacancy distribution (solid line) for the simulated defect profiles. Even if the vacancy distribution is not constant inside the layer, the *W*/*S* area and the integrated trapping fraction remain proportional (see Fig. 10), but the proportionality does not follow the linear relation corresponding to a constant defect profile. Sample 4 and its trapping fraction agree with the areas relationship as can be seen in Fig. 9.

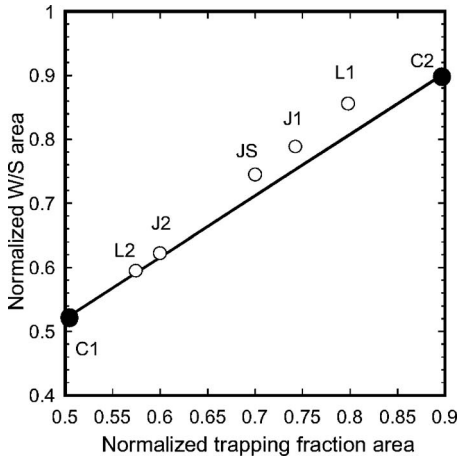

FIG. 10. Normalized *W*/*S* area versus normalized trapping fraction area. The solid line corresponds to constant vacancy profiles in the layer. The open circles correspond to the defect profiles defined in Table III and Fig. 7.

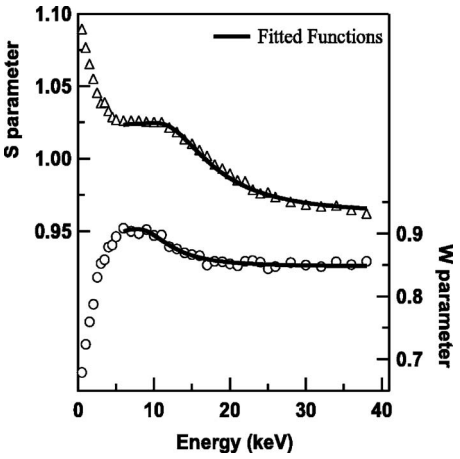

FIG. 11. Fit of the W and S curves, corresponding to sample 6, versus energy using Eq. (7).

E. Fit of the defect profile and the layer thickness

Considered the previous discussion, the variation of the trapping fraction η_{VZn} can be obtained fitting the W and S parameters versus the implantation energy simultaneously (see Fig. 11) using Eq. (7). We have divided each layer along its thickness in three different zones of the same size and constant trapping fraction. The zone closest to the interface is zone 3 and the one closest to the surface zone 1 (see Table IV). W and S parameters have been adjusted simultaneously in order to obtain the best fit and the layer thickness value has been left free. Low-energy W/S values have not been used in order to avoid the surface influence. The obtained layer thicknesses and the values of η_{VZn} along each zone are summarized in Table IV. The vacancy concentrations have been calculated assuming a positron trapping coefficient of zinc vacancies on the order of 3×10^{15} s^{-1} at 300 K.[7]

TABLE IV. Layer thicknesses calculated from the fit of W and S parameters versus positron energy with Eq. (5). $Z1$, $Z2$, and $Z3$ run from the surface to the interface, respectively (see text). Trapping fractions (η_{VZn}) and its corresponding vacancy concentrations (C_{VZn}) are also shown.

Sample	Calculated thickness (nm)	η_{VZn} [$C(V\text{Zn})$ (ppm)]		
		Zone 1	Zone 2	Zone 3
1	570±20	0.83(3) [10±2]	1.00(9) [>20]	1.0(1) [>20]
2	510±70	0.39(5) [1.3±0.3]	0.86(9) [12±9]	1.00(8) [>20]
3	450±20	0.64(2) [3.5±0.3]	1.00(8) [>20]	1.0(1) [>20]
4	920±30	0.45(2) [1.6±0.2]	0.64(4) [3.5±0.6]	1.00(5) [>20]
5	830±90	0.81(3) [8±2]	1.00(9) [>20]	1.0(1) [>20]
6	650±70	0.49(2) [1.6±0.2]	0.39(4) [1.3±0.2]	0.92(4) [20±10]
7	690±20	0.31(7) [0.9±0.3]	0.6(1) [3±1]	1.00(8) [>20]

The new values for the layers thicknesses are in average about 50 nm larger than the ones presented in Table II, and, except in the case of sample 5, they are in good agreement with thicknesses measured by SEM. The errors of the parameters presented in Table IV correspond to the statistical errors of the fitting procedure. But in samples 2, 5, and 6, the error bars correspond to the separation between the experimental points around the abandon point. The W/S value corresponding to the zinc vacancy reported previously[7] has been used, without taking into account its error bars.

However, as Fig. 8 shows, the error of such determination is large and in consequence there is a great difficulty for obtaining good quantitative values for the zinc vacancy trapping fraction η_{VZn}. Lines joining the substrate value and the error bars of the zinc vacancy value are drawn as a guide for the eye. All experimental values are situated above the lower line in Fig. 8. Therefore, a precise determination of the W/S point corresponding to the zinc vacancy will highly improve the quantitative values of trapping fractions and, at the same time, zinc vacancy concentrations. However, the defect profile trends presented on Table IV are not affected by the precise determination of the zinc vacancy W/S point, and therefore they are reliable.

As seen in Table IV, even though the slope of the vacancy concentration profile within the layer depends on the layer, in all the layers studied the concentration of zinc vacancies is maximum near the ZnO layer/sapphire interface. The increase is large, and in samples 1, 3, and 5 saturated trapping at defects is observed near the interface.

V. CONCLUSIONS

In this work we have presented a method to analyze the W/S plots of Doppler broadening data obtained with a slow positrons beam. In heteroepitaxial semiconductor layers, the method allows one to determine easily and nondestructively the thickness of the layer. The determination can be improved by increasing the W/S points measured at energies around the "abandon point." The method gives the possibility of making quantitative determinations of both the defect profile inside the layer and its thickness. The method has been used for characterizing ZnO layer/sapphire substrate heterostructures, but can be easily generalized to other heterostructures, homostructures, or materials with other sharp changes in the trapping characteristics of positrons, when there is no appreciable trapping at the interface states. We have shown that W/S plots have rich information, and an analysis of its characteristics can be of great interest to increase knowledge of the samples.

ACKNOWLEDGMENTS

The work has been undertaken under Projects No. MAT2003-406841, No. MAT2004-06841, No. MEC872/2006, No. GV ACOMP06/037, and No. UPV00224.310-144553/2002 and with the financial support of the MEC and Basque Government under the Researchers Formation Program.

*Electronic address: asier.zubiaga@ehu.es

[1] K. Saarinen, T. Laine, S. Kuisma, J. Nissilä, P. Hautojärvi, L. Dobrzynski, J. M. Baranowski, K. Pakula, R. Stepniewski, M. Wojdak, A. Wysmolek, T. Suski, M. Leszczynski, I. Grzegory, and S. Porowski, Phys. Rev. Lett. **79**, 3030 (1997).

[2] F. Tuomisto, V. Ranki, K. Saarinen, and D. C. Look, Phys. Rev. Lett. **91**, 205502 (2003).

[3] Z. Q. Chen, M. Maekawa, S. Yamamoto, A. Kawasuso, X. L. Yuan, T. Sekiguchi, R. Suzuki, and T. Ohdaira, Phys. Rev. B **69**, 035210 (2004).

[4] X. D. Pi, P. G. Coleman, T. L. Tseng, C. P. Burrows, B. Yavich, and W. N. Wang, J. Phys.: Condens. Matter **14**, L243 (2002).

[5] A. Uedono, T. Koida, A. Tsukazaki, M. Kawasaki, Z. Q. Chen, SF. Chichibu, and H. Koinuma, J. Appl. Phys. **93**, 2481 (2003).

[6] T. Koida, A. Uedono, A. Tsukazaki, T. Sota, M. Kawasaki, and S. F. Chichibu, Phys. Status Solidi A **12**, 2841 (2004).

[7] A. Zubiaga, F. Tuomisto, F. Plazaola, K. Saarinen, J. A. García, J. F. Rommeluere, J. Zúniga Pérez, and V. Múñoz Sanjosé, Appl. Phys. Lett. **86**, 042103 (2005).

[8] K. Saarinen, P. Hautojarvi, and C. Corbel, *Identification of Defects in Semiconductors* (Academic Press, New York, 1998).

[9] C. Munuera, J. Zúñiga Pérez, J. F. Rommeluere, V. Sallet, R. Triboulet, F. Soria, V. Múñoz Sanjosé, and C. Ocal, J. Cryst. Growth **264**, 70 (2004).

[10] A. van Veen, H. Schut, M. Clement, J. M. M. de Nijs, A. Kruseman, and M. R. Ijpma, Appl. Surf. Sci. **85**, 216 (1995).